EUROFUSION WPS2-PR(15) 13721

AM de Aguilera et al.

Magnetic well scan and confinement in the TJ-II sterllarator

Preprint of Paper to be submitted for publication in
Nuclear Fusion

This work has been carried out within the framework of the EUROfusion Consortium and has received funding from the Euratom research and training programme 2014-2018 under grant agreement No 633053. The views and opinions expressed herein do not necessarily reflect those of the European Commission.

Magnetic well scan and confinement in the TJ-II sterllarator

Adriana M. de Aguilera, Francisco Castejón, Enrique Ascasíbar, Emilio Blanco, Eduardo De la Cal, Carlos Hidalgo, Bing Liu, Antonio López-Fraguas, Francisco Medina, María Antonia Ochando, Ignacio Pastor, María Ángeles Pedrosa, Boudewijn Van Milligen, and the TJ-II Team

EUROfusion-Ciemat, Av Complutense 22. 28040 Madrid. Spain

(Dated: March 17, 2015)

Abstract

Magnetic well is the main stabilising mechanism in the TJ-II stellarator, since this is an almost shearless device. TJ-II has the capability to vary its magnetic configuration by changing the currents of its coils, allowing one to change the magnetic well keeping almost constant the vacuum rotational transform profile, in particular. This characteristic makes this stellarator a suitable device to study the impact of unfavourable magnetic well conditions on plasma performance and stability. The here reported experiments explored a family of ten magnetic configurations with similar rotational transform and varying magnetic well, from positive values to negative ones, hence exploring Mercier-unstable configurations. We succeeded in developing reproducible NBI-heated plasmas, even when the most Mercier-unstable configurations were performed, although the turbelnce level was higher in the latter configurations. The position of the plasma boundary agreed with the equilibrium calculations in all the cases.

I. INTRODUCTION

Stellarators are designed to present good Mercier stability properties, which is the case of TJ-II [1]. Besides Mercier criterion, stellarators are aimed to present a small Shafranov shift [2], stability to ballooning modes [3] and optimized neoclassical confinement properties [4]. Optimization under Mercier criterion has always some implications on the design of the device, making mandatory the conception of complex magnetic configurations with coils difficult to build and hence, expensive.

When one considers the perturbations that interchange magnetic flux between two regions of a plasma, the concept of magnetic well arises as a relevant property of magnetic configuration for this process. Magnetic Well measures plasma stability against short perpendicular wavelength modes driven by the plasma pressure gradient [5]. In the $\vec{J} \to 0$ (currentless) limit the magnetic well is defined as:

$$\hat{W} = 2\frac{V}{\langle B^2 \rangle}\frac{d}{dV}\left\langle \frac{B^2}{2} \right\rangle \tag{1}$$

Where $\langle B \rangle$ represents the averaged magnetic field for closed magnetic line in a closed magnetic surface.

Analyzing the magnetic flux through a magnetic surface, one concludes that the stability assessment for interchange modes includes the condition that the average magnetic field intensity on a magnetic surface is minimum, i.e., the stable plasma region is the one where the intensity of the magnetic field, B, increases, averaged on a magnetic surface, along the outward direction [6]. So, being the specific volume $U = dV/d\Phi$, and U_0 its value on the magnetic axis and U_a on the outermost surface, the magnetic well depth is:

$$\frac{-\Delta U}{U} = \frac{U_0 - U_a}{U_0} \tag{2}$$

Local stellarator stability is studied by using the Mercier criterion, which establishes that the plasma is stable when the energy interchange of tubes of plasma is positive. Therefore, the stability condition becomes a variational principle. The plasma is stable against localised interchange perturbations when the functional derivative of the energy functional against radially localized perturbations is positive [7]. This condition can be expressed as:

$$D_M(\rho) = D_W(\rho) + D_S(\rho) + D_I(\rho) + D_K(\rho) \geq 0 \tag{3}$$

This equation gives us the linear stability properties of local interchange modes. The two first terms in the RHS of Eq. (3) represent the contribution of the magnetic well and the magnetic shear, both with stabilizing character. The third term corresponds to the plasma current, whose stabilizing capability depends on its sign and on the possible introduction of resonances in the plasma column. The last one comes from the geodesic curvature, which presents areas stable or unstable. All the terms are functions of the magnetic surface and are, therefore, calculated at every radial position given by the effective radius ρ. The higher the value of (3), the more stable the plasma one gets.

Previous experiments on LHD have shown the capability of achieving high pressure plasmas beyond the Mercier stability criterion without a serious degradation of confinement [8]. A possible theoretical explanation of these phenomena is given in [9], where the non-linear plasma profile evolution itself tends to create a pressure profile that avoids the instability. The self-organization mechanisms between transport and gradients that could play a role here are shown experimentally in [10]. The idea is that Mercier criterion only gives information of linear stability, because a stable situation with plasma confinement is found, although nothing is said about the non-linear evolution of the plasma.

Further experiments on LHD have shown that magnetic well has also influence on island dynamics. The decreasing magnetic well tends to increase the island size, while the increasing one tends to heal the island [11]. High beta W7-AS plasmas were still stable under Mercier criterion (see e. g. [12]), since this device appeared to be stable for high beta plasmas.

TJ-II is an almost shearless device [13], therefore the main stabilising term in (3) is the corresponding to the magnetic well. Changing the magnetic well is a knob to modify the stability properties of the plasma. In a previous work, the effect of magnetic well scan on turbulent flux was investigated in ECRH low density plasmas, showing an increase of such flux, but without any remarkable impact on plasma confinement [14]. In the present work we explore the effects on plasma confinement of the reduction of the magnetic well taking advantage of the flexibility of TJ-II in NBI plasmas. TJ-II allows one to explore magnetic configurations with very low values of magnetic well and even, in some cases, with magnetic hill, but keeping similar rotational transform profiles around the plasma edge [1], so that the changes on stability properties depend only on the magnetic well scan.

This paper is organized as follows. Section II is devoted to explain the properties of the TJ-II stellarator, which makes this device appropriated for this study, and the analyzed

diagnostics. The Mercier criterion calculations come in Section III, and the experimental results are shown in Section IV. Section V is devoted to the Conclusions and the Discussion of the results.

II. EXPERIMENTAL SETUP

TJ-II is a heliac-type stellarator with an average major radius of $R = 1.5\ m$ and an average minor radius (for the standard configuration) of $a = 0.22\ m$ (see [13]). It is capable of confining plasmas lasting several hundreds of ms with a first ECRH heating phase with two 53.2 GHz gyrotrons that deliver $\approx 300\ kW$ in the second harmonic of X mode; and then a NBI heating phase during which each injector can provide up to 600 MW. Although TJ-II disposes of two NBI injectors, only one of them was available when the reported experiments were carried out.

As it has been stated above, TJ-II is an almost shearless stellarator: this feature allows one an accurate control of the low-order rational values that appear in the rotational transform profile and makes magnetic well its main stabilizing mechanism [3], [1]. This makes TJ-II a very suitable device to explore the stability thresholds by reducing the magnetic well profile for similar $\iota/2\pi$ profiles at the plasma edge. Figure 1 (a) shows the complete ten-configuration family that has been explored in these experiments. It covers a wide range of magnetic well conditions that cam be examined in Table I: starting with optimal stability conditions, with ascending positive well values along most of the plasma radius (configurations 100_44_64 to 100_44_77); then attempting cases with $W(\rho) > 0$ but $dW(\rho)/d\rho < 0$ for the outer plasma region $\rho > 0.8$ (from 100_44_84 to 99_44_90) and, finally, three configurations (from 100_43_99 to 100_41_109) with negative and decreasing magnetic well along most of the plasma column. In TJ-II, these numbers stand for the current that circulate for the magnetic field coils as in TF_VF_CC. Fig. 1 (b) provides the $\iota/2\pi$ profiles for all the mentioned configurations, proving that most of them exhibit the 8/5 rotational close to the $\rho \approx 0.8$ position.

For simplicity reasons, we will label the configurations with their magnetic well values at the plasma edge ($W(\rho = 1)$). Fig. 1 (c) shows a drastic reduction of plasma volume when we perform a scan decreasing the magnetic well value: the theoretically least stable configurations are almost half of the volume of the most stable ones. Fig. 2 shows three

Configuration	Magnetic Well (%)	Plasma Volume (m^3)
100_44_64	2.36	1.096
101_42_64	2.35	1.079
100_44_70	1.66	0.991
100_44_77	1.11	0.847
100_44_84	0.54	0.771
099_44_87	0.32	0.723
099_44_90	0.12	0.680
100_43_99	−0.29	0.568
100_42_104	−0.53	0.511
100_41_109	−0.69	0.450

TABLE I. List of magnetic configurations explored during the experiments. The Magnetic Well value is taken at $\rho = 1$,

examples of how the vacuum magnetic field lines topology and plasma size change from the bigger and almost symmetrical configurations (left) to the small and deformed low stability cases. It is also seen that more stable configurations are also more symmetric, with respect to the line that units the magnetic axis with the central conductor, than the less stable ones. These changes in topology are accompanied by the appearance of larger magnetic islands for the same magnetic perturbation introduced numerically in the configurations.

Turbulence at the plasma edge was studied using a rake-type Langmuir probe shown schematically in Fig. 3 (a) and in a photograph (taken between two of the experimental days) in Fig. 3 (b). The plasma sections shown in Fig. 2 correspond to the sector where the mentioned Langmuir probe is located, and the dotted lines that cross the field lines represent the access range of the probe for each configuration (also represented in a more general way in Fig. 3 (c)). The probe consists of eight pins separated by 1.7 mm along the radial direction as shown in the schematics of Fig. 3 (a). All the pins are set to measure floating potential of plasma with a 2 MHz sampling rate. Although the probe is at a fixed position during each plasma discharge, it can be displaced several times in order to measure floating potential profiles at different radial positions in the plasma periphery for similar density and temperature conditions.

III. THEORETICAL CALCULATIONS

Here we show the Mercier criterion calculations for the configuration 100_42_104 which has a magnetic well value in the edge of $W = -0.53\%$, therefore it is supposed to be unstable even for low pressure plasmas. As we will show in the following Section, we still obtain stable plasmas in such a configuration experimentally as well as in those with theoretically worse stability properties, which is an important result. Two types of pressure profiles are used for the calculations, linear and quadratic with the normalized magnetic flux (see Fig. 4 (a), where $s = \rho^2$).

The shapes of the magnetic surfaces of three magnetic configurations of the family considered for this work have been shown in Fig. 2, where the Poincaré maps of the field lines are shown. One can see in the Poincaré plots the onset of the rational 8/5 that appears at the minor radius $\rho \approx 0.8$. The shape of the configurations also changes strongly.

When equilibrium is calculated using VMEC [15], it is observed that the magnetic well is increased with plasma pressure and becomes larger for the quadratic profile. The plasma becomes more stable, as can be seen in figure Fig. 4 (b), for the vacuum case and for the former two types of pressure profile. Nevertheless this magnetic well increase is not enough to stabilize the configuration in the Mercier sense.

We perform the Mercier criterion calculation for the case of the linear pressure profile and $< \beta > \approx 0.3$ %, which is of the order of the values we have used in our experiments. The Mercier coefficient of Eq. 3, D_M, is negative along the whole minor radius and shows a large minimum at the position of the $\iota/2\pi = 8/5$ resonance, showing that the mode is strongly unstable, as can be seen Fig. 4 (c). The effect of this mode on global stability can be limited, since the fraction of the profile affected is small.

We perform a zoom of the Mercier coefficients (see Fig. 4 (d)) in order to explore the effect of the different terms. The large minimum is dominant, showing some radial extension. It can be seen that the Mercier coefficient D_M is negative along the whole minor radius, which implies that the plasma is unstable everywhere, despite of the fact that the magnetic well is positive in the inner radii. Having a detailed look on the figure, it is seen that the shear and the current terms are very small, as expected, while the most destabilising term is the geodesic curvature. Therefore, Mercier stability in TJ-II is a play between the stabilising magnetic well and destabilising geodesic curvature.

We find that the plasma is Mercier unstable even in the inner radii, where the magnetic well term is positive. Experiments have been performed to explore the effect of such instability on TJ-II plasmas.

IV. RESULTS

A. Stored energy and confinement time

The present results take into account tens of plasma discharges, with more than five reproducible plasmas obtained in all the magnetic configurations described in Section II. A set of diamagnetic loops allows us to measure the stored diamagnetic energy for all the cases [22] i. Taking into account that plasma volume decreases drastically as we move from the most Mercier-stable to the most unstable configurations, we study the evolution of the stored energy divided by the plasma volume (density of plasma stored energy) instead of the plasma energy itself. Fig. 5 shows the energy density for the NBI heating phase dividing the data in three subgroups of common NBI-density values in TJ-II. Stored diamagnetic energy for each density range was extracted shot by shot. The error bars correspond to the dispersion of these data for a given magnetic well value. The density of stored energy on magnetic well is weakly decreasing by the decrease of the magnetic well for these NBI-plasmas. The effect seems to be stronger for the negative values of the magnetic well, being more clear for the low and high density cases.

The decrease of volume and change of plasma shape along the magnetic well scan (shown in Fig. 1 (c)) affect the absorption of NBI power. The Monte-Carlo code FAFNER [16] has been used to perform simulations for three electron density values to estimate the absorbed power for six of the configurations used in these experiments. The absorbed power for the four remaining configurations was obtained via polynomial interpolation of the simulated data. The results are shown in Fig. 6, where it is seen that the deposited NBI power depends on plasma volume almost as much as it does on electron density. The NBI power deposited in the plasma is used to estimate the energy confinement time for each magnetic configuration:

$$\tau_E = \frac{E}{P_{absorbed} - dE/dt} \tag{4}$$

The energy confinement time is plotted in Fig. 7. A weak dependency of τ_E with the

magnetic well is seen, while the latter it is positive. Only a clear decrease of τ_E is appreciated in the last three configurations of the studied family, the most Mercier-unstable ones. This result is not in contradiction with the behavior of the density of stored energy shown in Fig. 5. The trend observed in Fig. 7 of increasing τ_E up to the configuration with magnetic well equals to 0.5 includes both, the magnetic well and the plasma volume, the latter increasing almost linearly with the former. According to ISS04 scaling law [17], the confinement time increases almost linearly with the volume, since the major radius is constant in this device and the confinement increases as the square of minor radius, which would explain the strong dependence shown in Fig. 6, in contrast with the weaker shown in Fig. 5. For configurations with magnetic well value larger than 0.5, the confinement improvement with the volume does not appear due to the fact that the effective ripple is much larger in the plasma edge of those configurations, making larger the neoclassical transport (see [18], [19] and [20]) and compensating the improvement of confinement due to the increase of volume.

B. Shear layer position

The Langmuir probe described in Section II was used to measure the floating potential profiles shown in Fig. 8 (a) when positioned at different locations between $\rho = 1$ and $\rho = 0.8$. These profiles were obtained using data of several reproducible discharges, therefore at similar conditions of electron density and stored energy during the NBI phase, but with the Langmuir probe at slightly different radial positions. For clarity, Fig. 8 (a) shows floating potential profiles for three representative cases of the ten configurations explored when the mean electron density is $n_e(0) = 2 \cdot 10^{-19}\ m^{-3}$. These profiles are formed by several (always more than five) individual profiles, each of them corresponds to a different Langmuir probe radial position when reproducible plasmas were obtained. The dotted lines represent the grade 3 polynomial adjusted to each case: the change in curvature (maximum) of this polynomial is taken as the shear layer position for the given configuration and density.

When several (more than five) different individual floating potential profiles are extracted for a magnetic configuration, the radial behavior of the profile is clear, and can be easily fitted to a $3rd$ degree polynomial (black dotted lines in Fig. 8 (a)) with regression coefficient $R^2 > 0.9$. This fit is accurate enough to take care of the change of curvature that determines the shear layer position for each configuration, which gives the plasma boundary position

[21]. The amount of points contained in a density range varies from one discharge to another, and this is taken into account by weighting the mean shear layer position and its dispersion for each configuration and density. This procedure is repeated for all the configurations at different electron density values and the obtained shear layer positions, which are compared with the last closed flux surface position predicted via VMEC simulations.

We present in Fig. 8 (b) the measured shear layer postions against the LCFS calculated with VMEC, showing a clear one to one linear dependency. Bigger (more Mercier-stable) plasmas present a farther Last Closed Flux Surface (LCFS) position (more negative) and are represented by the points in the left region of the graph, while in the smaller (less Mercier-stable) configurations the absolute position of the LCFS is closer to the plasma core and appear represented in the right part of the graph. The error bars come from the polynomial adjust uncertainty: all the experimental points that fall into the error bar of each polynomial maximum are averaged to give a shear layer position, with their dispersion is represented in the error bars. The linear dependency exhibited between the calculated and the experimental positiones means that the effect of reducing the magnetic well in limiting the plasma size is negligible, if any. The same analysis of floating potential profiles acquired in other sector of TJ-II and using different Langmuir probe gives the same result: the shear layer position is not affected by the reduction of magnetic well, even in magnetic hill conditions. This means that the possible effect of the magnetic well on the 8/5 rotational is nule or negligible.

C. Electromagnetic turbulence

Langmuir probes are also suitable diagnostics to measure the electrostatic turbulence. Now we know the shear layer position for each configuration and we can study the turbulence in the floating potential signals at this point with similar physical properties. We took the root mean square (RMS) of the mentioned signals as a measure of the electrostatic turbulence level and, again, analyzed its behavior for some fixed electron density values. The result of this study is shown in Fig. 9 (a). For the same pins and signals (meaning the same shear layer positions extracted using the method explained in Section IV B) a Fourier spectrum (without electron density distinction) has also been computed (shown in Fig. 9 (b)). Both analysis methods show a noticeable increase of the electrostatic turbulence, specially for the three last magnetic configurations (the ones with negative magnetic well at the edge).

Finally, in order to complete our results with the magnetic turbulence, we implemented a similar Fourier analysis for one of the arrays of Mirnov coils in TJ-II. A detailed study of all the cases, taking into account the heating conditions, leads to the appearance of a recurring mode in the signals, whose frequency descends from $\approx 160\ kHz$ in the Mercier-stable TJ-II standard configuration to $\approx 50\ kHz$ for the more unstable magnetic hill cases. This behavior is show in Figures 10 (b), (c) and (d) for three selected NBI discharges at the most Mercier stable configuration, a magnetic hill situation and a negative magnetic well configuration respectively. Fig. 10 (a) shows the Fourier analysis of the floating potential signals of the Langmuir probe for the same magnetic well scan, although some more configurations have been included in this figure. The results exposed in Fig. 10: the frequency of this electromagnetic mode decreases as the magnetic well value lowers. Also, in general, the power intensity of these modes seems to decrease slightly when the magnetic hill configurations are compared with the Mercier-stable ones.

V. CONCLUSIONS

This paper reports on the results of several experiments devoted to the variation of the magnetic well carried out in the TJ-II stellarator between 2013 and 2014. The family of magnetic configurations chosen presents the 8/5 rational close to the edge and very similar rotational transform profiles. The main result of our research is the operation of plasmas well above the Mercier stability threshold, even under magnetic hill conditions. This plasmas were not only obtained, but also repeatedly reproduced, giving similar properties. The shear layer position is detected with Langmuir probes at the same position where it was expected to be via VMEC simulations, which shows that the interchange instabilities do not play a relevant role for edge plasma confinement.

Also density of stored diamagnetic energy appears to be almost unaffected by the decrease of Mercier stability, although energy confinement time reduces when the magnetic well value becomes negative at the plasma edge. Nevertheless this reduction can be attributed to the decrease of plasma volume in the configurations with shallow well or hill. In fact, the International Stellarator Scaling Law [17] predicts roughly a linear dependence of the confinement with the volume in TJ-II. For large magnetic configurations, the increase of the magnetic ripple compensates this improvement.

Electrostatic turbulence measured at the plasma edge with Langmuir probes and magnetic turbulence measured using Mirnov coils show an increase of electromagnetic activity in the low magnetic well plasmas, as it had been previously reported in [14] for ECRH plasmas. The relationship between this increase in electromagnetic activity and the modest degradation of confinement for plasmas beyond the Mercier stability criterion is unclear yet. The most feasible explanation is that Mercier criterion only provides information about the linear properties of interchange mode stability, saying nothing about the non-linear evolution. Self-organization mechanisms between MHD modes and transport could explain the good confinement of Mercier unstable plasmas in TJ-II.

VI. ACKNOWLEDGEMENT

This work has been carried out within the framework of the EUROfusion Consortium and has received funding from the European Unions Horizon 2020 research and innovation programme under grant agreement number 633053. The views and opinions expressed herein do not necessarily reflect those of the European Commission.

---

[1] A Varias, C Alejaldre, A Lopez Fraguas, L García, BA Carreras, N Dominguez, and VE Lynch. Ideal mercier stability for the tj-ii flexible heliac. *Nuclear Fusion*, 30(12):2597, 1990.

[2] VD Shafranov. Magnetohydrodynamic theory of plasma equilibrium and stability in stellarators: Survey of results. *Physics of Fluids (1958-1988)*, 26(2):357–364, 1983.

[3] R Sánchez, JA Jiménez, L Garcia, and A Varias. Compressibility effects on ideal and resistive ballooning stability in the tj-ii heliac device. *Nuclear fusion*, 37(10):1363, 1997.

[4] Bernhard Seiwald, Sergei V Kasilov, Winfried Kernbichler, VN Kalyuzhnyj, Viktor V Nemov, V Tribaldos, and JA Jiménez. Optimization of energy confinement in the $1/\nu$ regime for stellarators. *Journal of Computational Physics*, 227(12):6165–6183, 2008.

[5] Jeffrey P Freidberg. *Ideal MHD*. Cambridge University Press, 2014.

[6] Kenro Miyamoto. *Plasma physics and controlled nuclear fusion*, volume 38. Springer, 2006.

[7] C Mercier. Study of the behaviour of magnetic field lines after perturbation of the toroidal field on magnetic surfaces. *Nuclear fusion*, 30(4):743, 1990.

[8] S Sakakibara, KY Watanabe, Y Suzuki, Y Narushima, S Ohdachi, N Nakajima, F Watanabe, L Garcia, A Weller, K Toi, et al. Mhd study of the reactor-relevant high-beta regime in the large helical device. *Plasma Physics and Controlled Fusion*, 50(12):124014, 2008.

[9] Katsuji Ichiguchi and Benjamin A Carreras. Multi-scale mhd analysis incorporating pressure transport equation for beta-increasing lhd plasma. *Nuclear Fusion*, 51(5):053021, 2011.

[10] C Hidalgo, C Silva, BA Carreras, B van Milligen, H Figueiredo, L García, MA Pedrosa, B Gonçalves, and A Alonso. Dynamical coupling between gradients and transport in fusion plasmas. *Physical review letters*, 108(6):065001, 2012.

[11] S Sakakibara, Y Narushima, Y Takemura, M Okamoto, KY Watanabe, Y Suzuki, S Ohdachi, K Ida, M Yoshinuma, K Tanaka, et al. Response of mhd stability to resonant magnetic perturbation in the large helical device. *Nuclear Fusion*, 53(4):043010, 2013.

[12] A Weller, M Anton, J Geiger, M Hirsch, R Jaenicke, A Werner, C Nührenberg, E Sallander, DA Spong, et al. Survey of magnetohydrodynamic instabilities in the advanced stellarator wendelstein 7-as. *Physics of Plasmas (1994-present)*, 8(3):931–956, 2001.

[13] Carlos Alejaldre, J Alonso, J Botija, A Perez Navarro, L Garcia, A Lopez-Fraguas, et al. Tj-ii project: a flexible heliac stellarator. *Fusion Technol*, 17(1):131–139, 1990.

[14] J. Castellano, J. A. Jiménez, C. Hidalgo, M. A. Pedrosa, A. L. Fraguas, I. Pastor, J. Herranz, C. Alejaldre, and TJ-II Team. Magnetic well and instability thresholds in the tj-ii stellarator. *Physics of Plasmas*, 9(2):713–716, 2002.

[15] Steven P Hirshman and JC Whitson. Steepest-descent moment method for three-dimensional magnetohydrodynamic equilibria. *Physics of Fluids (1958-1988)*, 26(12):3553–3568, 1983.

[16] A Teubel, J Guasp, and M Liniers. Monte carlo simulations of nbi into the tj-ii helical axis stellarator. *Report IPP*, 4(268):264, 1994.

[17] H Yamada, JH Harris, A Dinklage, E Ascasibar, F Sano, S Okamura, J Talmadge, U Stroth, A Kus, S Murakami, et al. Characterization of energy confinement in net-current free plasmas using the extended international stellarator database. *Nuclear fusion*, 45(12):1684, 2005.

[18] CD Beidler and William NG Hitchon. Ripple transport in helical-axis advanced stellarators: a comparison with classical stellarator/torsatrons. *Plasma physics and controlled fusion*, 36(2):317, 1994.

[19] W Dommaschk, W Lotz, and J Nührenberg. Monte-carlo simulation of neoclassical transport in stellarators. *Nuclear fusion*, 24(6):794, 1984.

[20] F Castejón, A Gómez-Iglesias, MA Vega-Rodríguez, JA Jiménez, JL Velasco, and JA Romero. Stellarator optimization under several criteria using metaheuristics. *Plasma Physics and Controlled Fusion*, 55(1):014003, 2013.

[21] C Hidalgo, JH Harris, T Uckan, JD Bell, BA Carreras, JL Dunlap, GR Dyer, Ch P Ritz, AJ Wootton, MA Meier, et al. Plasma fluctuations near the shear layer in the atf torsatron. *Nuclear fusion*, 31(8):1471, 1991.

[22] VD Pustovitov. Diamagnetic measurements and plasma energy in toroidal systems. *Plasma Physics and Controlled Fusion*, 52(8):085005, 2010.

LIST OF FIGURES

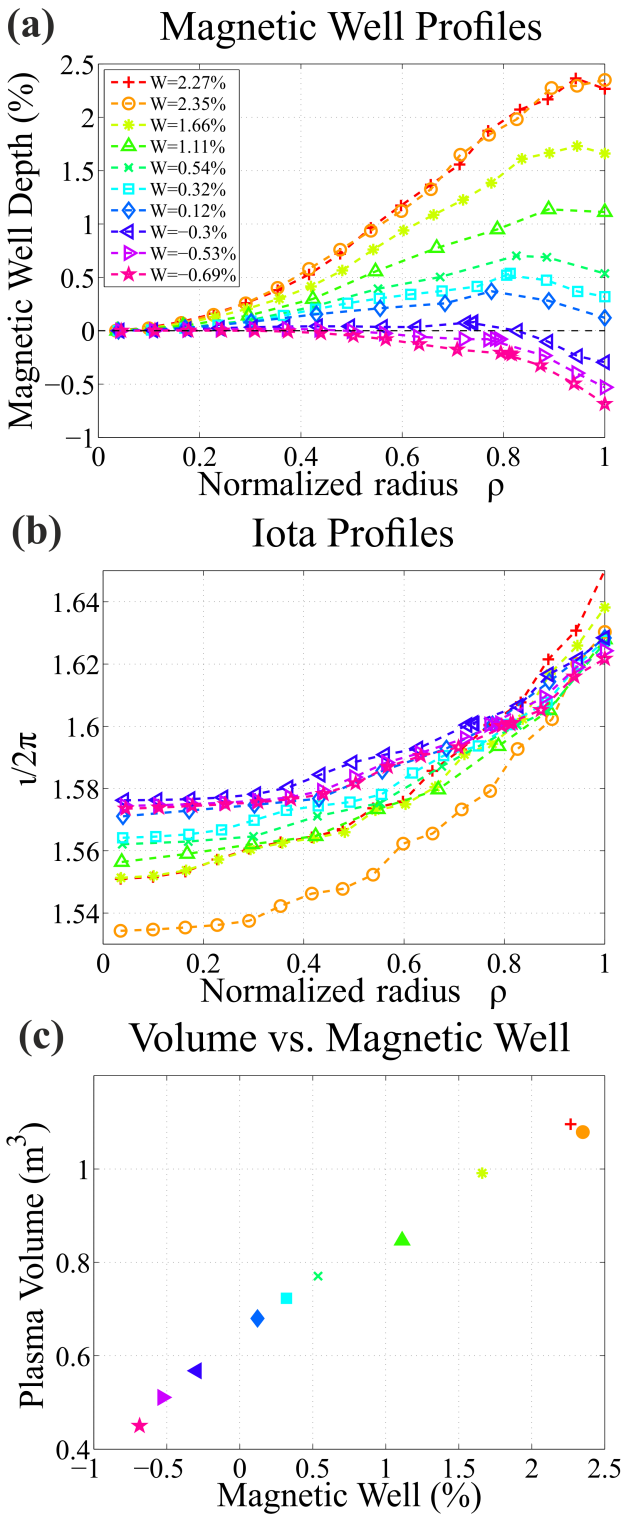

FIG. 1. *The same legend applies for the three figures:* **(a)** *Magnetic well radial profile.* **(b)** *Rotational transform along normalized radius. The 8/5 rational can be clearly seen around* $\rho \approx 0.8$ *in all the cases.* **(c)** *Volume for each configuration.*

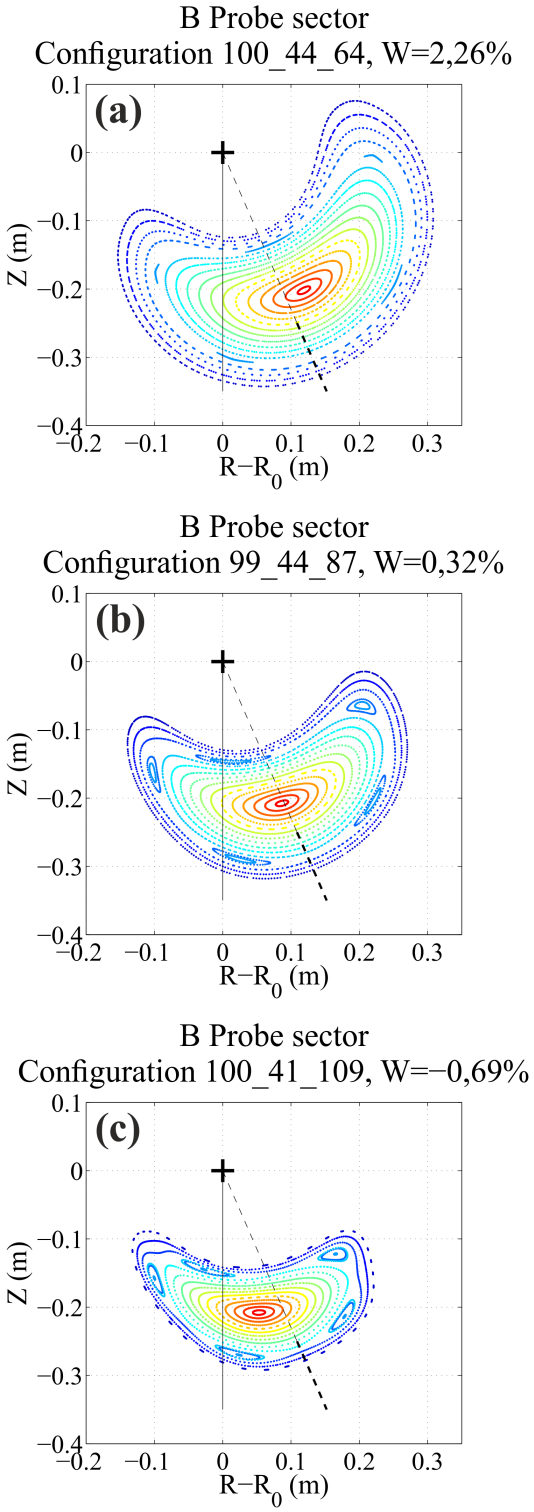

FIG. 2. *Poincar plots of the magnetic field lines for three of the explored configurations. The magnetic island is created artificially by introducing a magnetic perturbation.*

FIG. 3. *Langmuir probe:* **(a)** *Schematics of the probe system.* **(b)** *Recent photograph of the rake of pins.* **(c)** *Plasma access region.*

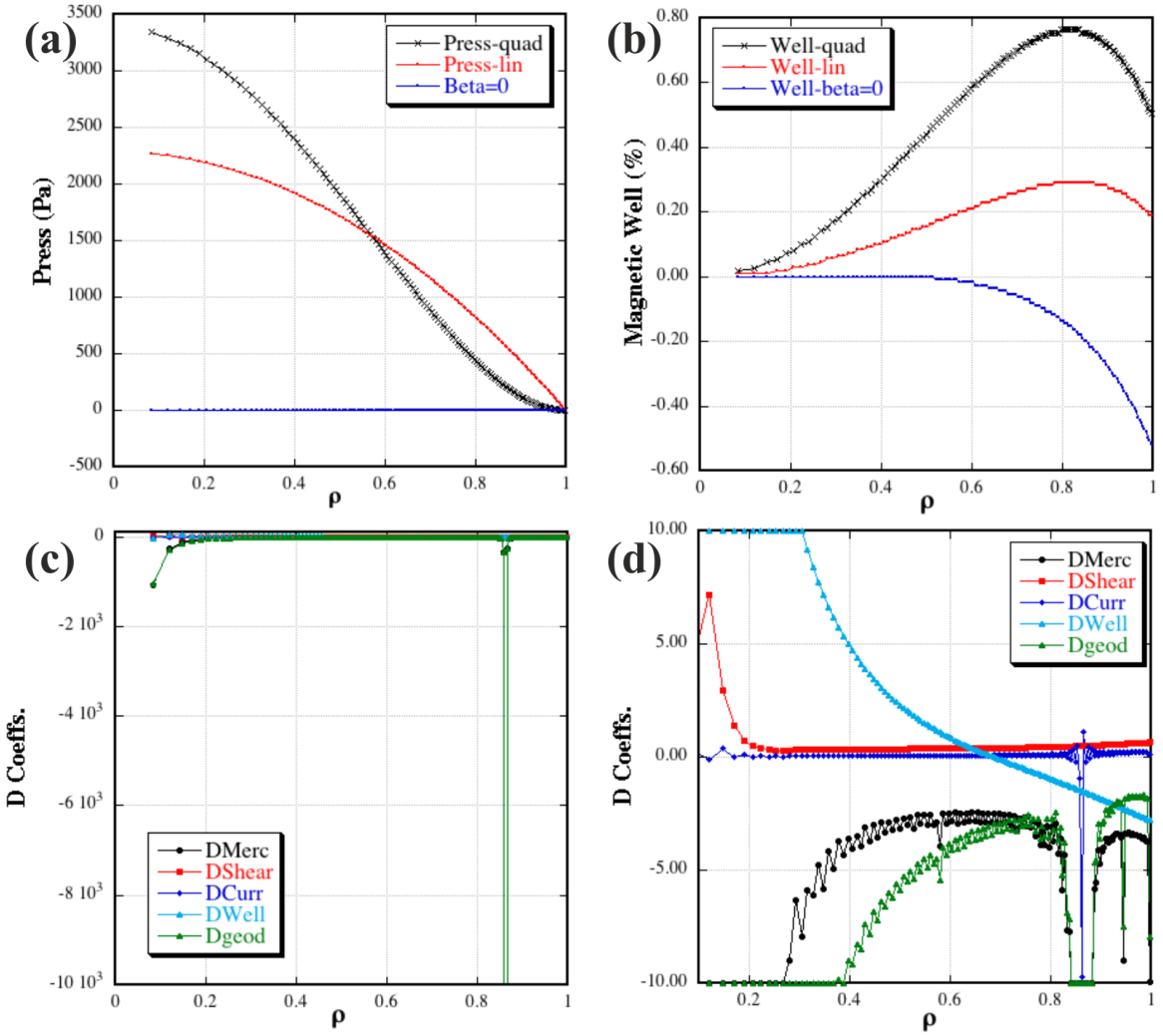

FIG. 4. *For the* 100_42_104 *configuration, with* $W = -0.53$ % **(a)** *Pressure profiles with the flux used in the calculations.* **(b)** *Magnetic well profile calculated when the previous pressure profiles are taken into account.* **(c)** *Calculated Mercier coefficients for the linear pressure profile.* **(d)** *Zoom on the (c) panel to explore the behaviors of the Mercier terms and the* $\iota/2\pi = 8/5$ *resonance area.*

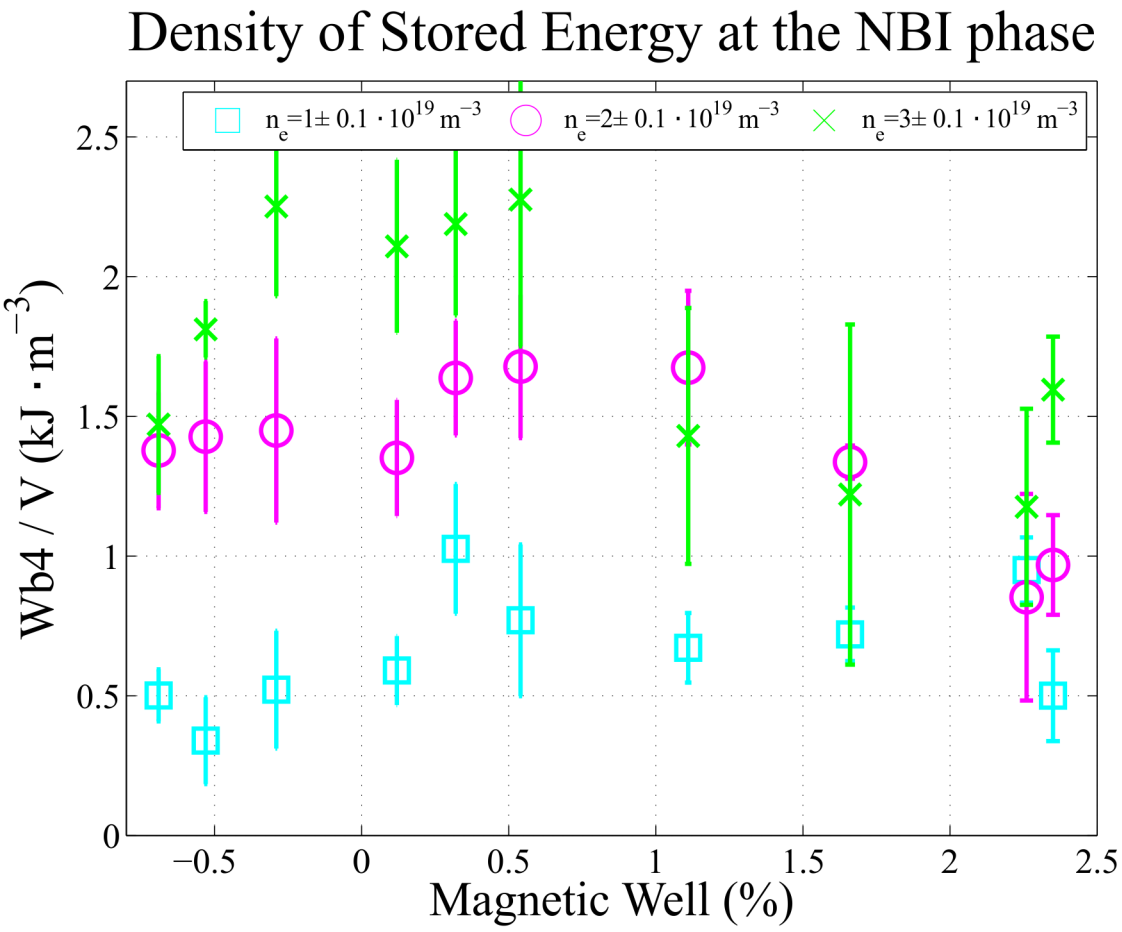

FIG. 5. *Density of stored diamagnetic energy during NBI heating with respect to the magnetic well for three density values. It is only affected by the low magnetic well conditions for low density stages.*

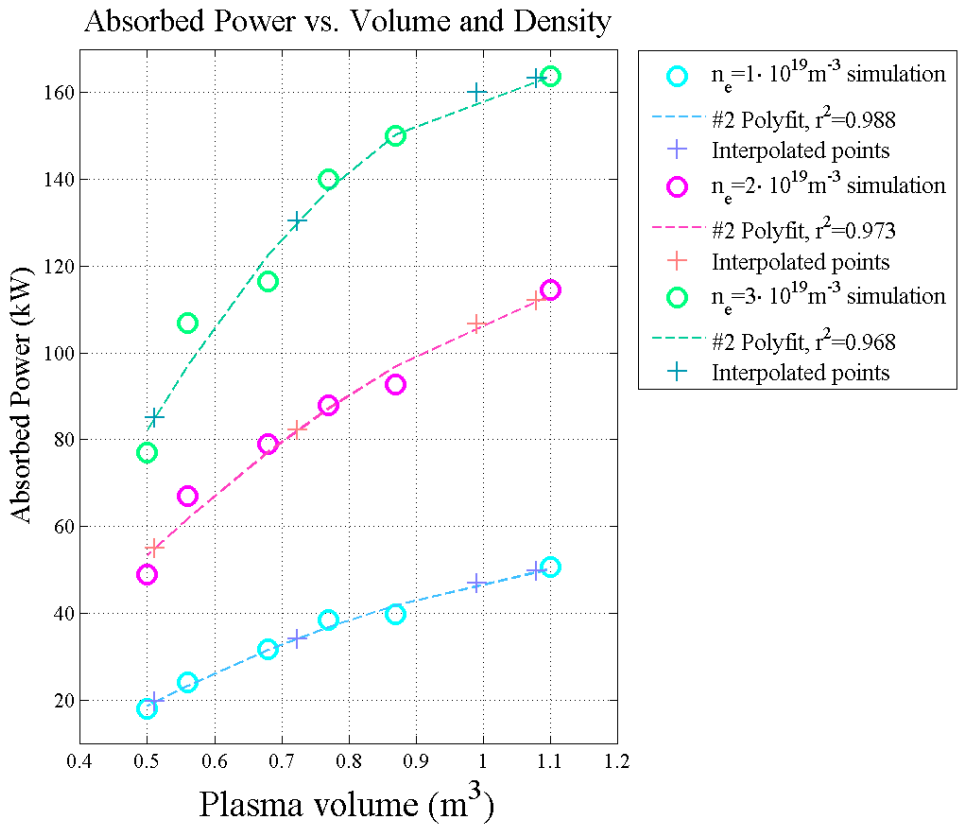

FIG. 6. *NBI absorbed power (Fafner simulation) for three possible electron densities,* $n_e(0) = 1$, *2 and 3* $\cdot 10^{19} m^{-3}$ *for different plasma volumes. Non simulated configurations were adjusted by a parabolic fit.*

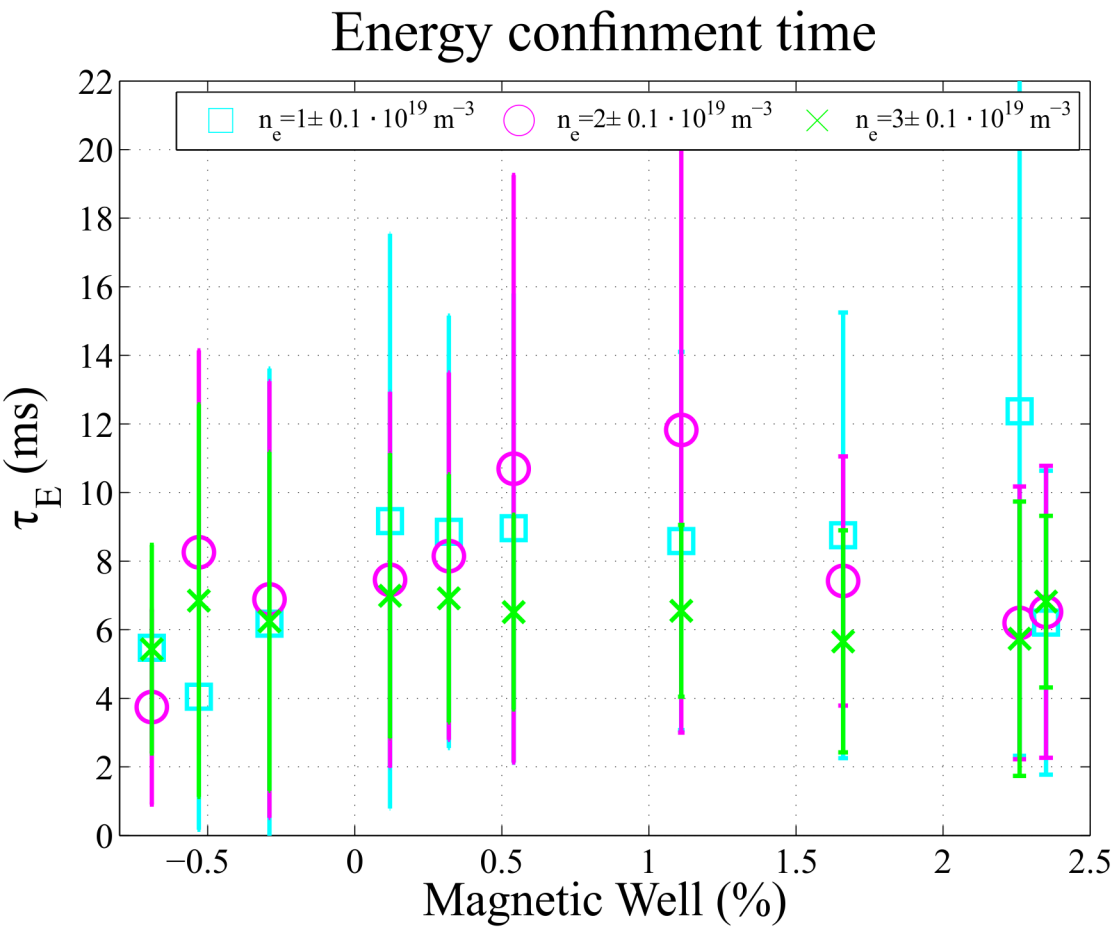

FIG. 7. *Energy confinement time for three fixed electron density values shows little dependency on magnetic well.*

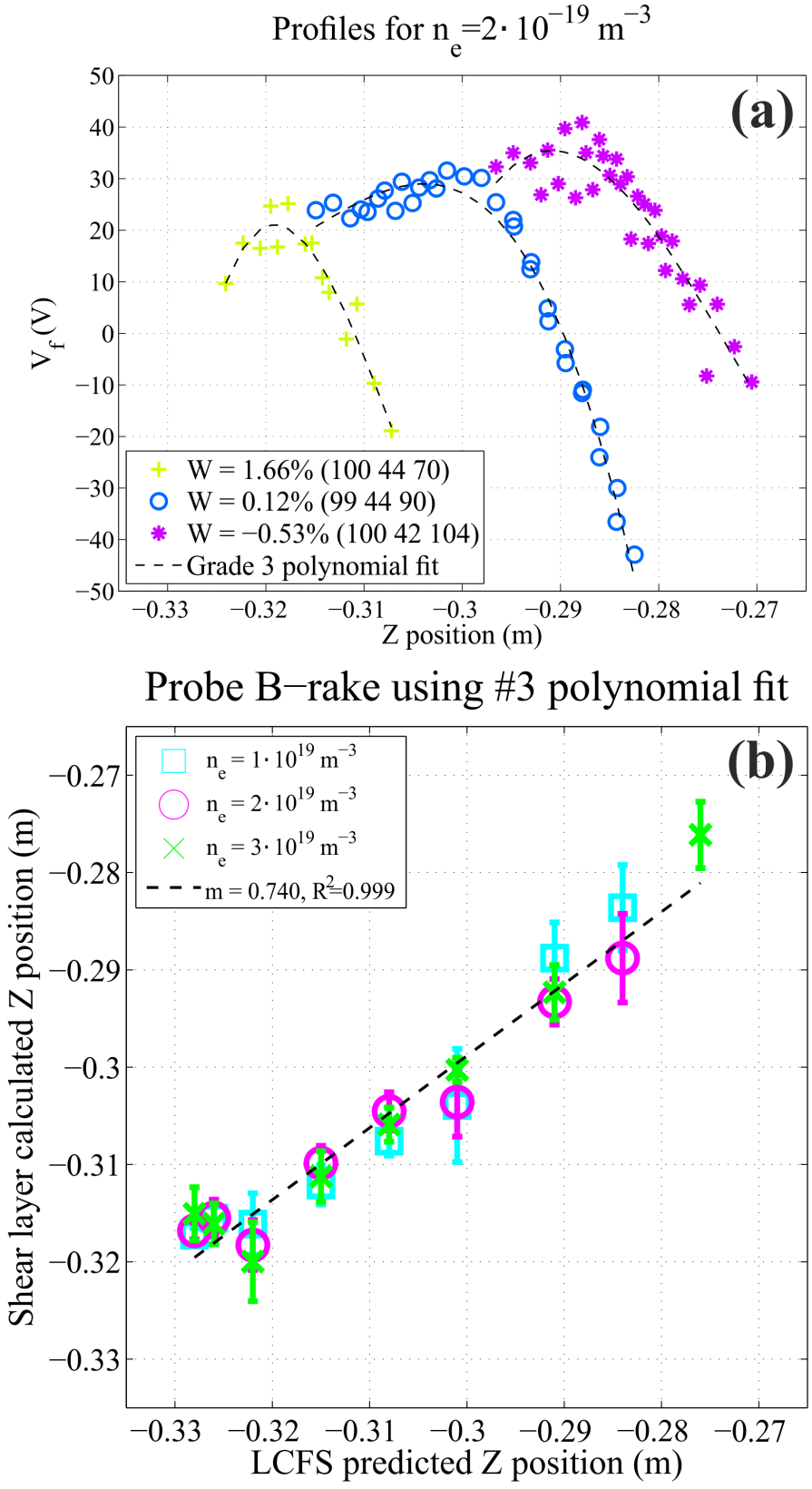

FIG. 8. **(a)** *Selected floating potential profiles for* $n_e(0) = 2{\cdot}10^{19}m^{-3}$ *as built in Sec. IV B.* **(b)** *The shear layer position of each configuration lies where the LCFS was predicted by VMEC calculations.*

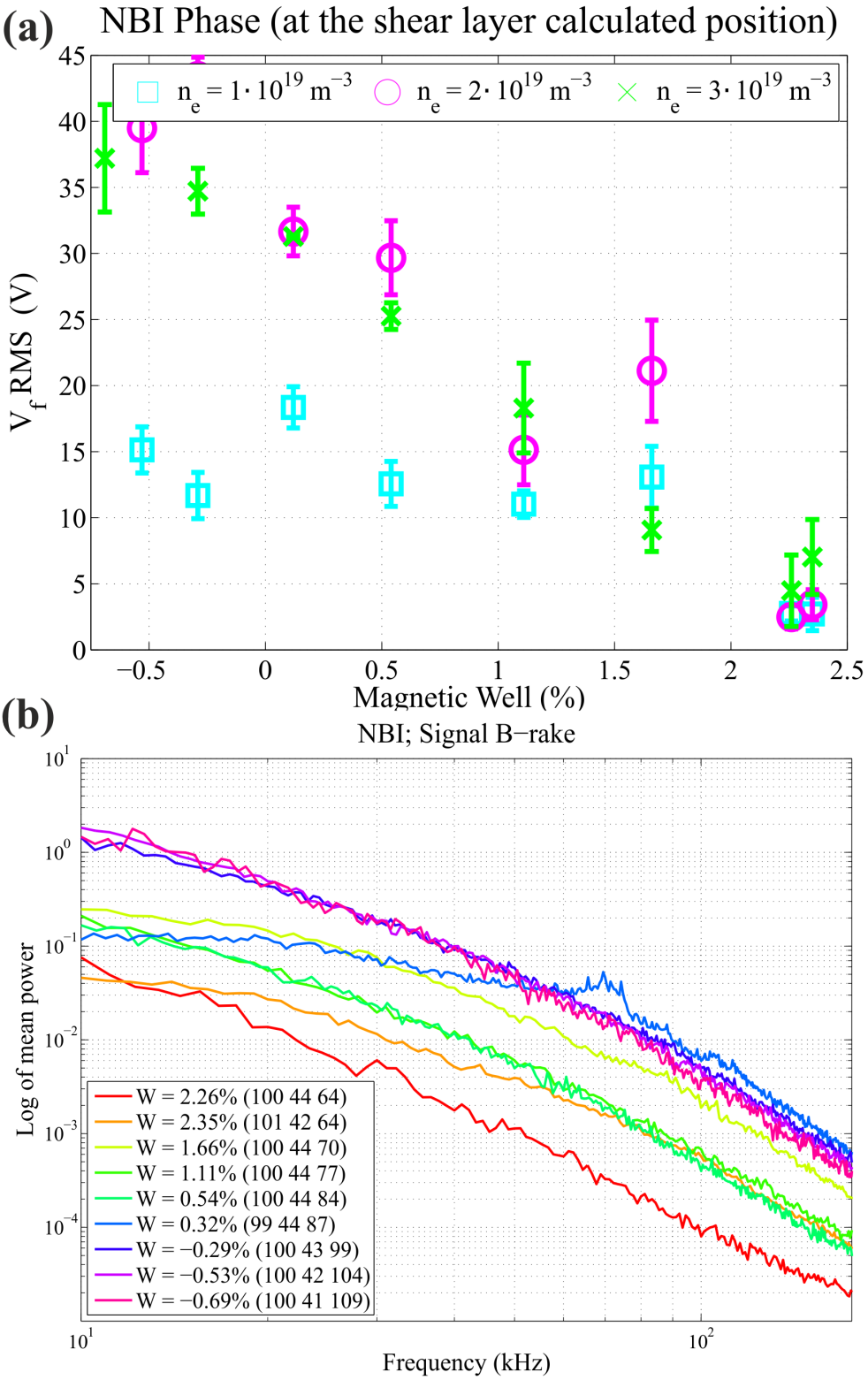

FIG. 9. **(a)** *RMS of the floating potentials at the shear layer extracted position for each configuration during the NBI heating phase.* **(b)** *Fourier spectrum of the floating potential power for the calculated shear layer positions (same pins and signals shown in* **(a)**.

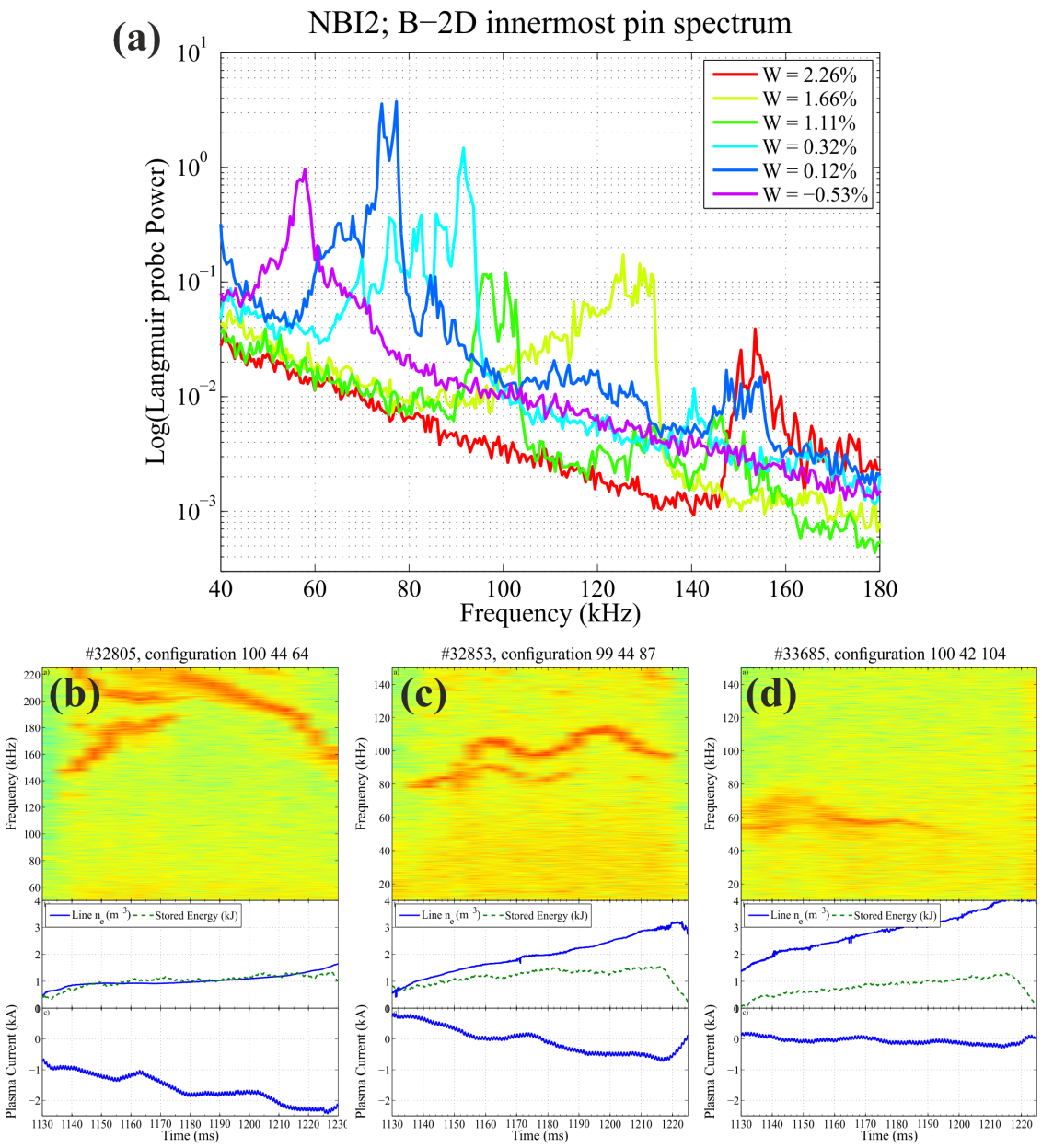

FIG. 10. *Electromagnetic spectrum.* **(a)** *Fourier analysis of the floating potential of selected inner radial positions at the Langmuir probe for several configurations of the magnetic well scan. A peak with decreasing frequency as we go to Mercier-unstable situations can be appreciated in all the cases. For* **(b)**, **(c)** *and* **(d)** *Mirnov coil power spectrum, electron density, diamagnetic stored energy and plasma current for three selected plasma discharges in the* $W = 2,24$ *%* **(b)**, $W = 0,32$ *%* **(c)** *and* $W = -0,53$ *%* **(d)** *configurations. A similar frequency decreasing mode can be seen in these magnetic signals, pointing to a electromagnetic nature of this phenomena.*